United States Geological Survey Earthquake Hazards Program

Final Technical Report

USGS Award Number G15AP00052

Characterization of crustal faulting in southern Alaska using moment tensors derived from full seismic waveforms

Carl Tape

University of Alaska Fairbanks
Geophysical Institute
903 Koyukuk Dr.
Fairbanks, AK 99775
Phone: 907-474-5456
Fax: 907-474-7290
Email: ctape@alaska.edu

Other personnel:
Vipul Silwal, University of Alaska Fairbanks, PhD student
Anthony Lomax, ALomax scientific

Award term: 4/1/2015 to 3/31/2016 (NCE to 3/31/2017)

Abstract

Several large ($M \geq 6$) earthquakes have occurred in the vicinity of Anchorage, Alaska, within the past century. The presence of the underlying subducting Pacific plate makes it difficult to determine the origin of these older earthquakes as either crustal, slab, or the subduction plate interface. We perform a seismological study of historical and modern earthquakes witin the Cook Inlet and Susitna region, west of Anchorage. We first estimate hypocenters for historical large earthquakes in order to assess the likelihood as crustal, slab, or plate interface. We then examine modern crustal seismicity to better understand the style of faulting and the location of active structures, including within (and beneath) Cook Inlet and Susitna basins. We perform double-couple moment tensor inversions using high frequency body waves (1–10 Hz) for small to moderate ($M \geq 2.5$) crustal earthquakes (depth $\leq$ 30 km) occurring from 2007 to 2017. Our misfit function combines both waveforms differences as well as first-motion polarities in order to obtain reliable moment tensor solutions. Three focus regions—Beluga, upper Cook Inlet, and Susitna—exhibit predominantly thrust mechanisms for crustal earthquakes, indicating an overall compressive regime within the crust that is approximately consistent with the direction of plate convergence. Mechanisms within upper Cook Inlet have strike directions aligned with active anticlines previously identified in Cook Inlet from active-source seismic data. Our catalog of moment tensors is helpful for identifying and characterizing subsurface faults from seismic lineaments and from faults inferred from subsurface images from active-source seismic data.

1 Introduction

The active tectonics of south-central Alaska is governed primarily by the northwestern subduction of the Pacific plate beneath the North America plate (Figure 1). The setting is one of the most seismically active regions in the world, having produced the M_{w} 9.2 1964 earthquake. It includes pervasive earthquakes in the slab, down to depths of 200 km, as well as crustal seismicity spanning a broad zone of intraplate deformation (Figure 2) (*Page et al.*, 1991; *Bird*, 2003). Many of the earthquakes—both large and small—are not clearly associated with any geologically mapped active faults. With improved locations of earthquakes and improved characterization of the style of faulting from these earthquakes, we can better assess the active faults in the region. Here we perform a seismological study of a tectonically complex region of south-central Alaska to improve our understanding of active tectonics and seismic hazards in the region.

The Pacific plate subducts to the northwest under south-central Alaska (Figure 1a). Attached to the Pacific plate to the east is the Yakutat microplate, identified as an oceanic plateau that is colliding and subducting beneath Alaska (*Plafker et al.*, 1978; *Eberhart-Phillips et al.*, 2006; *Christeson et al.*, 2010). The subducting Pacific/Yakutat plate is interpreted to be responsible for the extremely shallow angle of subduction ($< 5°$), far inland, as well as for the lack of volcanism *Eberhart-Phillips et al.* (2006); *Rondenay et al.* (2010).

We focus on the Cook Inlet and Susitna region, which spans the western margin of the Pacific/Yakutat plate (Figure 1a). The region, outlined in Figure 1, contains several notable tectonic elements. The subduction interface (*Li et al.*, 2013) exhibits a clear kink from a westward-dipping slab to a northwestern-dipping slab (*Ratchkovski and Hansen*, 2002) (Figure 1a). The interface ranges from a depth of 40 km in the southeast, beneath the Kenai peninsula, to a depth of 100 km in the northwest, beneath the Alaska Range. The southeast corner also marks the approximate downdip extent of the 1964 M_{w} 9.2 earthquake (*Davies et al.*, 1981; *Ichinose et al.*, 2007). Slow

slip and tectonic tremor have been identified on the deeper sections of the interface, from about 40 km to 80 km (*Ohta et al.*, 2006; *Wei et al.*, 2012; *Fu and Freymueller*, 2013; *Li et al.*, 2016). The crustal thickness inferred from receiver functions is ∼30 km in the northern region (*Veenstra et al.*, 2006), implying that these deeper slow slip events would arise from contact with subcrustal mantle.

The dynamics of underlying subduction provide context for characterizing crustal structures and crustal earthquakes, which are the target of this study. Within the Cook Inlet and Susitna region are two mapped active faults: the Castle Mountain fault and the Pass Creek fault. The Pass Creek fault is a normal fault extending 40 km (*Haeussler et al.*, 2017). The Susitna section of the Castle Mountain fault is >120 km and is part of a 500-km-long fault system extending to Lake Clark in the southwest and into the Talkeetna mountains to the northeast (*Koehler et al.*, 2012). Physiographically the Cook Inlet and Susitna region is marked by the presence of two major sedimentary basins: the Cook Inlet basin south of the Castle Mountain fault, and the Susitna basin north of the fault (Figure 1b)). These basins are surrounded by mountains: Talkeetna mountains to the east, Alaska Range to the northwest, Tordrillo mountains to the west, and Kenai mountains to the south. Additional faults and folds have been identified within 3D active-source seismic data in Cook Inlet and Susitna basins (*Bruhn and Haeussler*, 2006; *Lewis et al.*, 2015; *Haeussler et al.*, 2017).

We conduct a seismological study that spans three different methods and three sets of earthquakes in the Cook Inlet and Susitna region. First, in Section 2 we estimate the hypocenters of the largest earthquakes ($M_{\mathrm{w}} \geq 5.8$) that have occurred since the start of the instrumental era in 1904 (*Gutenberg and Richter*, 1954). We use globally recorded arrival times of P and S waves, in addition to traveltime predictions in a spherically symmetric Earth model, within a probabilistic inversion for hypocenter and origin time. Second, in Section 3 we use P waveforms and first-motion polarities to estimate focal mechanisms for crustal earthquakes$M_{\mathrm{w}} \geq 2.5$. This procedure is challenging on account of the lack of large earthquakes that are available. Third, we relocate seismicity ($M \geq 1.5$, 1990–2017) using arrival time data and a double-difference relocation algorithm (*Waldhauser and Ellsworth*, 2000). The results from these three analyses reveal a predominance of thrust faulting in the crust, consistent with structural inferences from subsurface images, but differing from the strike-slip mechanisms previously estimated from large historical earthquakes. Widespread seismicity and different styles of faulting provide challenges for characterizing different scenarios for future large earthquakes in this region.

2 Hypocenter estimation of historical earthquakes

At least 12 major events ($M_{\mathrm{w}} \geq 5.8$) have been originated in the Cook Inlet and Susitna region since the start of instrumental era in 1904. For larger earthquakes we use the Global Centroid Moment Tensor (GCMT) catalog (*Dziewonski et al.*, 1981; *Ekström et al.*, 2012) for events since 1976 and the ISC-GEM catalog (*Storchak et al.*, 2013; *International Seismological Centre*, 2018) for events before 1976. The ISC-GEM catalog provides relocated hypocenters (*Engdahl et al.*, 1998; *Bondár and Storchak*, 2011) and magnitude estimates (*Giacomo et al.*, 2015). In recent years, it has expanded its coverage of historical earthquakes to lower magnitudes. Doser and colleagues have estimated hypocenters, magnitudes, and mechanisms for many historical earthquakes in south-central Alaska (*Doser*, 2006, 2005; *Doser and Brown*, 2001; *Flores and Doser*, 2005).

We use a nonlinear probabilistic approach to estimate the hypocenters of the 11 pre-1976 earth-

quakes $M_w \geq 5.8$ in the region. The code, NonLinLoc, uses an efficient global sampling algorithm to obtain an estimate of the probability density function (pdf) in 3D space for the hypocenter location. The pdf (and the likelihood) is computed using the misfit between the observed and theoretical arrival times for teleseismic stations. Theoretical travel times are computed for spherical earth with `ak135` velocity model (*Kennett et al.*, 1995) using TauPToolkit *Crotwell et al.* (1999). Recorded arrival times are obtained from the International Seismological Centre (*International Seismological Centre*, 2015).

Our full results for all 11 historical earthquakes are presented in *Lomax et al.* (2018); next we highlight three of the largest earthquakes.

2.1 The 1933, 1943, and 1954 earthquakes

We present results from three $M_w > 6$ earthquakes in the Cook Inlet and Susitna region: 1933-04-27 M_w 6.8, 1943-11-03 M_w 7.3, and 1954-10-03 M_w 6.4. These earthquakes were widely felt across south-central Alaska, including Kodiak, and at least as far north as Fairbanks, which is about 400 km from the epicenters.

The seismicity cross sections in Figure 2b-c provide context for these three earthquakes. The plots show our maximum likelihood (MLL) hypocenters for the three earthquakes in the context of modern seismicity and estimated subsurface interfaces (subduction and Moho). From these results alone, it appears that the 1933 and 1943 earthquakes are crustal, while the 1954 earthquake was likely intraslab, though we cannot rule out the subduction interface as a possibility.

Station coverage and traveltime residuals for our MLL hypocenters (and origin times) are shown in *Lomax et al.* (2018). Figure 3 shows our posterior epicenters for the three earthquakes. These 'clouds' are approximately 30 km by 40 km and convey the uncertainty associated with the epicenter estimation. For each posterior hypocenter we calculate its vertical distance to the subduction interface, and these differences are then plotted as histograms in the bottom row of Figure 4. These distributions provide critical uncertainties for the interpretation of the earthquakes as crustal, subduction interface, or intraslab. For example, Figure 4c (bottom) makes the case for the 1954 earthquake as intraslab. (However, note that we do not have uncertainties for the subduction geometry models, including the one we have chosen to use (*Li et al.*, 2013)).

3 Moment tensor inversions for modern crustal earthquakes

We examine three catalogs of moment tensors: (a) *Doser and Brown* (2001): large $M_w > 6$ historical (pre-1964) earthquakes; (b) the GCMT catalog (*Dziewonski et al.*, 1981; *Ekström et al.*, 2012): post-1976 earthquakes, predominantly $M_w > 5.3$; (c) crustal earthquakes from the Alaska Earthquake Center fault-plane catalog: predominantly $M_l > 3$. Within the Cook Inlet and Susitna region, we see two historical crustal earthquakes (1933, 1943) and virtually no crustal earthquakes since 1976 (GCMT). Focal mechanisms for crustal earthquakes since 1990 are available from Alaska Earthquake Center. The mechanisms are estimated from first-motion polarities, and they vary widely across the region. Our primary motivation was to use enhanced methods, including waveforms, and enhanced station coverage from the past decade, to estimate moment tensors.

3.1 Event selection for moment tensor inversions

We consider earthquakes in the Cook Inlet and Susitna region shallower than 30 km and occurring between 2007-08-15 and 2017-01-01. From the spatial distribution of crustal seismicity, we identified three subregions to select events for moment tensor inversions: Beluga region, Upper Cook

Inlet region, and Susitna region (Table 1). The time period of event selection, 2007–2017, spans two seismic experiments in the region: MOOS (2007–2009) (*Li et al.*, 2013; *Abers and Christensen*, 2006) and SALMON (2015–2017) (*Tape et al.*, 2017, 2015) and also includes new stations from the EarthScope Transportable Array (TA) in Alaska (2014–2019). Station coverage is a primary factor on the reliability of our moment tensor solutions. Events in 2010, following the end of MOOS, have poor station coverage. Events starting in 2015 have the best coverage due to SALMON and TA networks.

We selected 53 events for moment tensor inversions: 9 from the Beluga region, 22 from the Upper Cook Inlet region, and 22 from the Susitna region. Hypocenters and origin times were obtained from the AEC catalog. These were fixed for the moment tensor inversions. Analyst-reviewed P arrival times and polarities were used for stations in the permanent network. For stations in temporary networks (MOOS, SALMON), we picked the P arrival times and assigned polarities.

3.2 Moment tensor inversion method

We use the 'cut-and-paste' approach to estimate moment tensors for earthquakes (*Zhao and Helmberger*, 1994; *Zhu and Helmberger*, 1996; *Zhu and Rivera*, 2002). In this approach, each three-component seismogram is cut into two body wave windows and three surface wave windows. Different bandpass filters are applied to the body waves and surface waves. The same procedures are applied to synthetic seismograms, which are then quantifiably compared with the recorded seismograms, via a misfit function. As demonstrated in *Silwal and Tape* (2016), the choices within the misfit function can have a significant impact on the estimated best-fitting moment tensor. Our previous studies (*Silwal and Tape*, 2016; *Alvizuri and Tape*, 2016) employed a simplified treatment of first-motion polarities that is generalized here.

3.3 Results

Figure 5 shows our estimated moment tensors for all 53 earthquakes spanning the three regions (Table 1). All three regions exhibit predominantly thrust-fault mechanisms. This includes several events within the epicentral region of the 1933 and 1943 crustal earthquakes (Figure 3). Interestingly, the previously published mechanisms for these two earthquakes indicate strike-slip (not thrust) faulting. Multiple explanations could be invoked to explain this discrepancy.

4 Project status

All seismological analyses for the project—including double-difference relocation of hypocenters (Figure 6)—have been completed. We are currently interpreting our results in the context of previous geological and seismological studies. Our intent is to submit a manuscript soon (*Silwal et al.*, 2018).

Publications from this work

1. *Silwal and Tape* (2017): Presentation at 2017 EarthScope meeting
2. *Lomax et al.* (2018): Catalog and results for hypocenters of historical earthquakes
3. *Silwal* (2018): Catalog and results for mechanisms of modern crustal earthquakes
4. *Silwal et al.* (2018): Manuscript in preparation for *Tectonophysics*

References

Abers, G., and D. Christensen (2006), Seismic and geodetic imaging of subducting terranes under North America, International Federation of Digital Seismograph Networks. Other/Seismic Network. doi:10.7914/SN/YV_2006.

Alvizuri, C., and C. Tape (2016), Full moment tensors for small events ($M_w < 3$) at Uturuncu volcano, Bolivia, *Geophys. J. Int.*, *206*, 1761–1783, doi:10.1093/gji/ggw247.

Amante, C., and B. W. Eakins (2009), ETOPO1 1 Arc-Minute Global Relief Model: Procedures, Data Sources and Analysis, NOAA Technical Memorandum NESDIS NGDC-24, 19 pp.

Bird, P. (2003), An updated digital model of plate boundaries, *Geochem. Geophy. Geosyst.*, *4*, 1027, doi:10.1029/2001GC000252.

Bondár, I., and D. Storchak (2011), Improved location procedures at the International Seismological Centre, *Geophys. J. Int.*, *186*, 1220–1244, doi:10.1111/j.1365-246X.2011.05107.x.

Bruhn, R. L., and P. J. Haeussler (2006), Deformation driven by subduction and microplate collision: Geodynamics of Cook Inlet basin, Alaska, *Geol. Soc. Am. Bull.*, *118*(3/4), 289–303.

Christeson, G. L., S. P. S. Gulick, H. J. A. van Avendonk, L. L. Worthington, R. S. Reece, and T. L. Pavlis (2010), The Yakutat terrane: Dramatic change in crustal thickness across the Transition fault, Alaska, *Geology*, *38*(10), 895–898.

Crotwell, H. P., T. J. Owens, and J. Ritsema (1999), The TauP Toolkit: Flexible Seismic travel-time and ray-path utilities, *Seismol. Res. Lett.*, *70*(2), 154–160.

Davies, J., L. Sykes, and K. Jacob (1981), Shumagin seismic gap, Alaska Peninsula: History of great earthquakes, tectonic setting, and evidence for high seismic potential, *J. Geophys. Res.*, *86*(B5), 3821–3855.

Doser, D. I. (2005), Historical seismicity (1918-1964) of the kodiak island region, *Bull. Seismol. Soc. Am.*, *95*(3), 878–895, doi:10.1785/0120040175.

Doser, D. I. (2006), Relocations of earthquakes (1899–1917) in south-central alaska, *Pure and Applied Geophysics*, *163*(8), 1461–1476, doi:10.1007/s00024-006-0085-3.

Doser, D. I., and W. A. Brown (2001), A study of historic earthquakes of the Prince William Sound, Alaska, Region, *Bull. Seismol. Soc. Am.*, *91*(4), 842–857.

Dziewonski, A., T.-A. Chou, and J. H. Woodhouse (1981), Determination of earthquake source parameters from waveform data for studies of global and regional seismicity, *J. Geophys. Res.*, *86*(B4), 2825–2852, doi:10.1029/JB086iB04p02825.

Eberhart-Phillips, D., D. H. Christensen, T. M. Brocher, R. Hansen, N. A. Ruppert, P. J. Haeussler, and G. A. Abers (2006), Imaging the transition from Aleutian subduction to Yakutat collision in central Alaska, with local earthquakes and active source data, *J. Geophys. Res.*, *111*, B11303, doi:10.1029/2005JB004240.

Ekström, G., M. Nettles, and A. M. Dziewoński (2012), The global GCMT project 2004–2010: Centroid-moment tensors for 13,017 earthquakes, *Phys. Earth Planet. Inter.*, *200-201*, 1–9, doi: 10.1016/j.pepi.2012.04.002.

Engdahl, E. R., and A. Villasenor (2002), Global seismicity: 1900–1999, in *International Handbook of Earthquake and Engineering Seismology*, *International Geophysics Series*, vol. 81A, edited by W. H. K. Lee, H. Kanamori, P. C. Jennings, and C. Kisslinger, pp. 665–690, Academic Press, London.

Engdahl, E. R., R. van der Hilst, and R. Buland (1998), Global teleseismic earthquake relocation with improved travel times and procedures for depth determination, *Bull. Seismol. Soc. Am.*, *88*(3), 722–743.

Flores, C., and D. I. Doser (2005), Shallow seismicity of the Anchorage, Alaska, Region (1964-1999), *Bull. Seismol. Soc. Am.*, *95*(5), 1865–1879, doi:10.1785/0120040121.

Fu, Y., and J. T. Freymueller (2013), Repeated large Slow Slip Events at the south central Alaska subduction zone, *Earth Planet. Sci. Lett.*, *375*, 303–311.

Giacomo, D. D., I. Bondár, D. A. Storchak, E. R. Engdahl, P. Bormann, and J. Harris (2015), ISC-GEM: Global instrumental earthquake catalogue (1900–2009), III. re-computed MS and mb, proxy MW, final magnitude composition and completeness assessment, *Physics of the Earth and Planetary Interiors*, *239*, 33–47, doi:10.1016/j.pepi.2014.06.005.

Gutenberg, B., and C. F. Richter (1954), *Seismicity of the Earth and Associated Phenomena*, 2 ed., Princeton U. Press, Princeton, New Jersey, USA.

Haeussler, P. J., R. W. Saltus, R. G. Stanley, N. Ruppert, K. Lewis, S. M. Karl, and A. Bender (2017), The peters hills basin, a neogene wedge-top basin on the broad pass thrust fault, south-central alaska, *Geosphere*, *13*(5), 1464–1488, doi:10.1130/ges01487.1.

Hayes, G. P., D. J. Wald, and R. L. Johnson (2012), Slab1.0: A three-dimensional model of global subduction zone geometries, *J. Geophys. Res.*, *117*, B01302, doi:10.1029/2011JB008524.

Ichinose, G., P. Somerville, H. K. Thio, R. Graves, and D. O'Connell (2007), Rupture process of the 1964 Prince William Sound, Alaska, earthquake from the combined inversion of seismic, tsunami, and geodetic data, *J. Geophys. Res.*, *112*, B07306, doi:10.1029/2006JB004728.

International Seismological Centre (2015), On-line Bulletin, `http://www.isc.ac.uk`, Internatl. Seis. Cent., Thatcham, United Kingdom (accessed 2017-05-03).

International Seismological Centre (2018), ISC-GEM Global Instrumental Earthquake Catalogue, Version 5.0, released on 2018-02-27.

Jadamec, M. A., and M. I. Billen (2010), Reconciling surface plate motions with rapid three-dimensional mantle flow around a slab edge, *Nature*, *465*, 338–342, doi:10.1038/nature09053.

Kennett, B. L. N., E. R. Engdahl, and R. Buland (1995), Constraints on seismic velocities in the Earth from traveltimes, *Geophys. J. Int.*, *122*, 108–124.

Kirschner, C. E. (1988), Map Showing Sedimentary Basins of Onshore and Continental Shelf Areas, Alaska, U.S. Geol. Survey Miscellaneous Investigation Series I-1873.

Koehler, R. D., R.-E. Farrell, P. A. C. Burns, and R. A. Combelick (2012), Quaternary faults and folds in Alaska: A digital database, doi:10.14509/23944, Alaska Div. Geol. Geophys. Surv. Miscellaneous Publication 141, 31 p., 1 sheet, scale 1:3,700,000.

Lewis, K. A., C. J. Potter, A. K. Shah, R. G. Stanley, P. J. Haeussler, and R. W. Saltus (2015), Preliminary Interpretation of Industry Two-Dimensional Seismic Data from Susitna Basin, South-Central Alaska, doi:10.3133/ofr20151138, U.S. Geol. Survey open-file report 2015-1138.

Li, J., G. A. Abers, Y. Kim, and D. Christensen (2013), Alaska megathrust 1: Seismicity 43 years after the great 1964 Alaska megathrust earthquake, *J. Geophys. Res.*, *118*, 4861–4871, doi:10.1002/jgrb.50358.

Li, S., J. Freymueller, and R. McCaffrey (2016), Slow slip events and time-dependent variations in locking beneath Lower Cook Inlet of the Alaska-Aleutian subduction zone, *J. Geophys. Res. Solid Earth*, *121*, 1060–1079, doi:10.1002/2015JB012491.

Lomax, A., V. Silwal, and C. Tape (2018), Hypocenter estimation for 14 earthquakes in south-central Alaska (1929–1975), ScholarWorks@UA at `http://hdl.handle.net/11122/8380`: descriptor file and zipped set of text files for each earthquake.

Ohta, Y., J. T. Freymueller, S. Hreinsdóttir, and H. Suito (2006), A large slow slip event and the depth of the seismogenic zone in the south central Alaska subduction zone, *Earth Planet. Sci. Lett.*, *247*, 108–116.

Page, R. A., N. N. Biswas, J. C. Lahr, and H. Pulpan (1991), Seismicity of continental Alaska, in *Neotectonics of North America*, edited by D. B. Slemmons, E. R. Engdahl, M. D. Zoback, and D. D. Blackwell, The Geology of North America, chap. 4, pp. 47–68, Geol. Soc. Am., Boulder, Colo., USA, Decade Map Volume 1.

Plafker, G., T. L. Hudson, T. Bruns, and M. Rubin (1978), Late Quaternary offsets along the Fairweather fault and crustal plate interactions in southern Alaska, *Can. J. Earth Sci.*, *15*(5), 805–816.

Ratchkovski, N. A., and R. A. Hansen (2002), New evidence for segmentation of the Alaska subduction zone, *Bull. Seismol. Soc. Am.*, *92*(5), 1754–1765.

Rondenay, S., L. G. J. Montési, and G. A. Abers (2010), New geophysical insight into the origin of the Denali volcanic gap, *Geophys. J. Int.*, *182*, 613–630.

Shellenbaum, D. P., L. S. Gregersen, and P. R. Delaney (2010), Top Mesozoic unconformity depth map of the Cook Inlet Basin, Alaska, doi:10.14509/21961, Alaska Div. Geol. Geophys. Surv. Report of Investigation 2010-2, 1 sheet, scale 1:500,000, available at `http://www.dggs.alaska.gov/pubs/id/21961` (last accessed 2016-10-30).

Silwal, V. (2018), Seismic moment tensor catalog for crustal earthquakes in the Cook Inlet and Susitna region of southern Alaska, ScholarWorks@UA at `http://hdl.handle.net/11122/8383`: descriptor file, text file of catalog, figures with waveform fits, and input weight files.

Silwal, V., and C. Tape (2016), Seismic moment tensors and estimated uncertainties in southern Alaska, *J. Geophys. Res. Solid Earth*, *121*, 2772–2797, doi:10.1002/2015JB012588.

Silwal, V., and C. Tape (2017), Crustal earthquakes in the Cook Inlet and Susitna regions, southern Alaska, Abstract presented at 2017 EarthScope National Meeting, Anchorage, Alaska, May 16-18.

Silwal, V., C. Tape, and A. Lomax (2018), Crustal earthquakes in the Cook Inlet and Susitna region of southern Alaska, *Tectonophysics* (in prep).

Storchak, D. A., D. Di Giacomo, I. Bondár, E. R. Engdahl, J. Harris, W. H. K. Lee, A. Villasenor, and P. Bormann (2013), Public release of the ISC–GEM Global Instrumental Earthquake Catalogue (1900–2009), *Seismol. Res. Lett.*, *84*(5), 810–815, doi:10.1785/0220130034.

Tape, C., D. H. Christensen, and M. M. Driskell (2015), Southern Alaska Lithosphere and Mantle Observation Network, International Federation of Digital Seismograph Networks. Other/Seismic Network. `doi:10.7914/SN/ZE_2015`.

Tape, C., D. Christensen, M. M. Moore-Driskell, J. Sweet, and K. Smith (2017), Southern Alaska Lithosphere and Mantle Observation Network (SALMON): a seismic experiment covering the active arc by road, boat, plane, and helicopter, *Seismol. Res. Lett.*, *88*(4), 1185–1202, doi:10.1785/0220160229.

Veenstra, E., D. H. Christensen, G. A. Abers, and A. Ferris (2006), Crustal thickness variation in south-central Alaska, *Geology*, *34*(9), 781–784.

Waldhauser, F., and W. L. Ellsworth (2000), A double-difference earthquake location algorithm: Method and application to the Northern Hayward fault, California, *Bull. Seismol. Soc. Am.*, *90*(6), 1353–1368, doi:10.1785/0120000006.

Wang, Y., and C. Tape (2014), Seismic velocity structure and anisotropy of the Alaska subduction zone derived from surface wave tomography, *J. Geophys. Res. Solid Earth*, *119*, 8845–8865, doi:10.1002/2014JB011438.

Wei, M., J. J. McGuire, and E. Richardson (2012), A slow slip event in the south central Alaska Subduction Zone and related seismicity anomaly, *Geophys. Res. Lett.*, *39*, L15309, doi:10.1029/2012GL052351.

Wickens, A. J., and J. H. Hodgson (1967), Computer Re-Evaluation of Earthquake Mechanism Solutions, Publications of the Dominion Observatory, Vol. 33, No. 1, Ottawa, Canada Department of Energy, Mines, and Resources, Contribution 103 to the International Upper Mantle Project.

Zhao, L.-S., and D. V. Helmberger (1994), Source estimation from broadband regional seismograms, *Bull. Seismol. Soc. Am.*, *84*(1), 91–104.

Zhu, L., and D. Helmberger (1996), Advancement in source estimation techniques using broadband regional seismograms, *Bull. Seismol. Soc. Am.*, *86*(5), 1634–1641.

Zhu, L., and L. A. Rivera (2002), A note on the dynamic and static displacements from a point source in multilayered media, *Geophys. J. Int.*, *148*, 619–627, doi:10.1046/j.1365-246X.2002.01610.x.

Table 1: Earthquake selection for three target subregions and for the full region. N_e is the number of earthquakes analyzed in each region for a particular method.

Region	longitude min (°)	longitude max (°)	latitude min (°)	latitude max (°)	method	N_e	max depth (km)	min mag	date range
Beluga region	-151.50	-151.10	61.25	61.90	moment tensor	9	30	M_l 2.5	2007-08-15 2017-01-01
Upper Cook Inlet region	-151.50	-150.60	60.60	61.25	moment tensor	22	30	M_l 2.5	2007-08-15 2017-01-01
Susitna region	-151.10	-149.90	61.50	62.50	moment tensor	22	30	M_l 3.0	2007-08-15 2017-01-01
Cook Inlet and Susitna region	-151.75	-149.50	60.50	62.50	historical	12	200	M_w 5.8	1904-01-01 2017-01-01
	-152.00	-149.00	60.50	62.50	double difference	5726	30	M_l 1.5	1990-01-01 2017-01-01

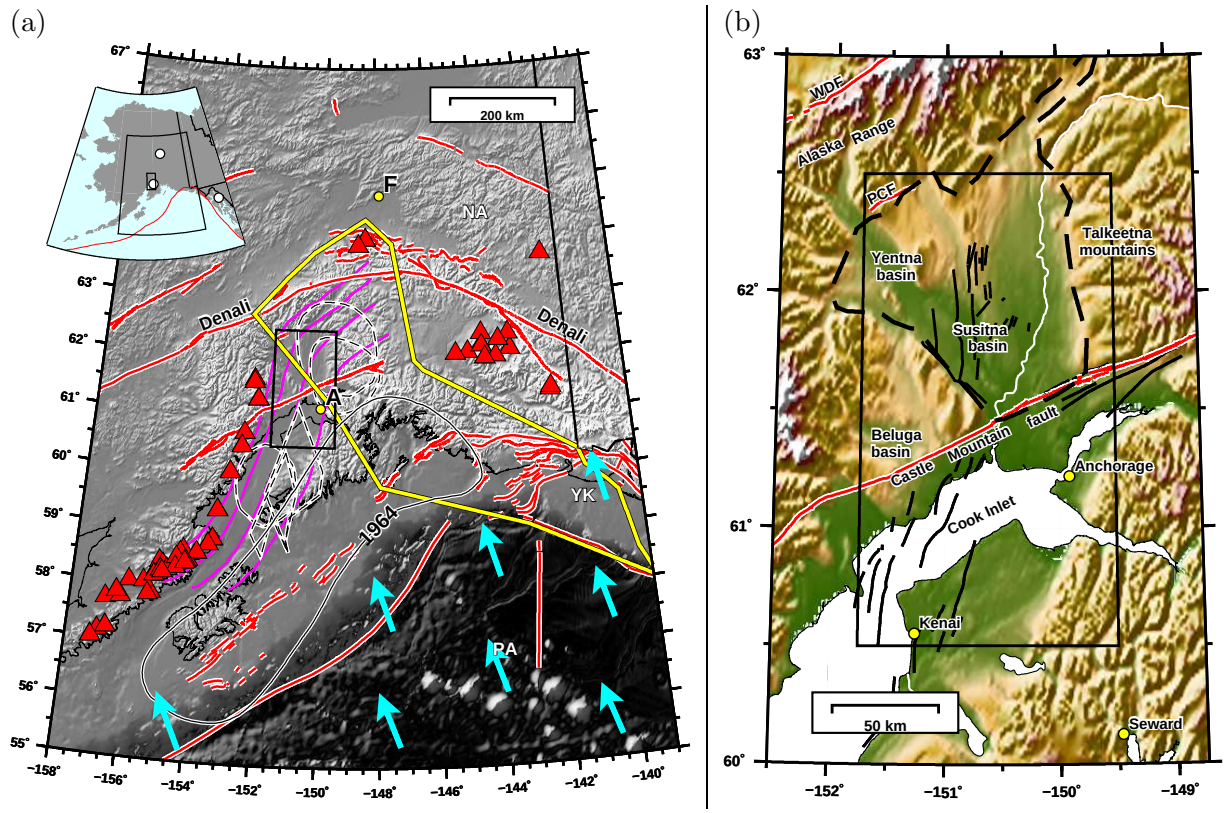

Figure 1: (a) Active tectonic setting of the Aleutian–Alaskan subduction zone, south-central Alaska. The rectangle in the middle shows the main study region. Cyan arrows shows the plate vectors for the subducting Pacific plate (PA) under the North American plate (NA) (*Bird*, 2003). Magenta curves are the 40 km, 60 km, 80 km, and 100 km contours of the top of the Pacific plate (*Li et al.*, 2013). Yellow bounded region denotes the surface and subsurface extent of the Yakutat block (YK) (*Eberhart-Phillips et al.*, 2006). Red triangles represent active volcanoes. Black dashed lines are inferred slows slip from various sources (*Ohta et al.*, 2006; *Wei et al.*, 2012; *Fu and Freymueller*, 2013; *Li et al.*, 2016). Also marked is the aftershock zone of the 1964 M_w 9.2 earthquake. Labeled cities: Anchorage (A) and Fairbanks (F). (b) Physiographic map of the Cook Inlet and Susitna region, south-central Alaska. Active faults are plotted in red and include Castle Mountain, Pass Creek (PCF) and the western Denali fault (WDF) at upper left (*Koehler et al.*, 2012). Other active faults (*Haeussler et al.*, 2017) and folds (*Koehler et al.*, 2012) are marked in black. Sedimentary basins are labeled: Cook Inlet, Susitna, Yentna, and Beluga. Cook Inlet basin underlies Cook Inlet and the western Kenai peninsula (*Shellenbaum et al.*, 2010). Black dashed lines are the boundaries of Susitna basin from *Kirschner* (1988).

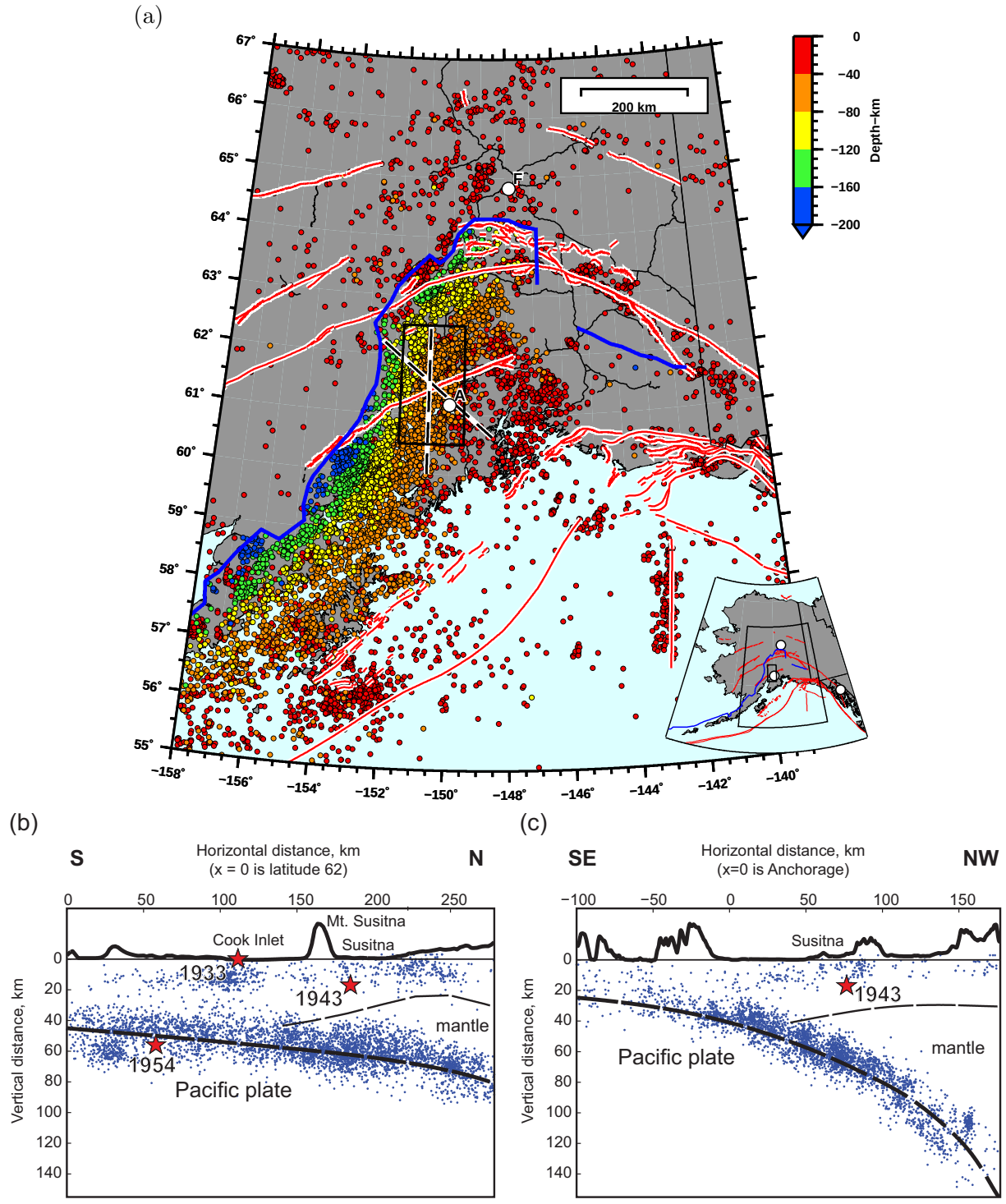

Figure 2: Seismicity in south-central Alaska. (a) Alaska Earthquake Center (AEC) catalog: $M_w \geq 2$, 1990-01-01 to 2017-01-01, colored by depth. The box, containing Anchorage (A), is the focus region of this study; the two profiles are shown in (b) and (c). The red lines are the active faults from *Koehler et al.* (2012). The blue line is the lateral extent of slab seismicity, digitized from the full AEC catalog. (b) S–N cross-section of (a) along the longitude line of −150.75°. Seismicity within 20 km of the profile is shown. Three large earthquakes of interest are projected onto the profile: 1933 M_w 6.78, 1943 M_w 7.34, and 1954 M_w 6.36; the hypocenters are estimated from NonLinLoc. Geometric boundaries shown are the plate interface (*Li et al.*, 2013), the Moho (*Wang and Tape*, 2014), and topography (*Amante and Eakins*, 2009) exaggerated by a factor of 20. (c) SE–NW cross-section of (a) between Anchorage ($x = 0$ km) and the 1943 earthquake.

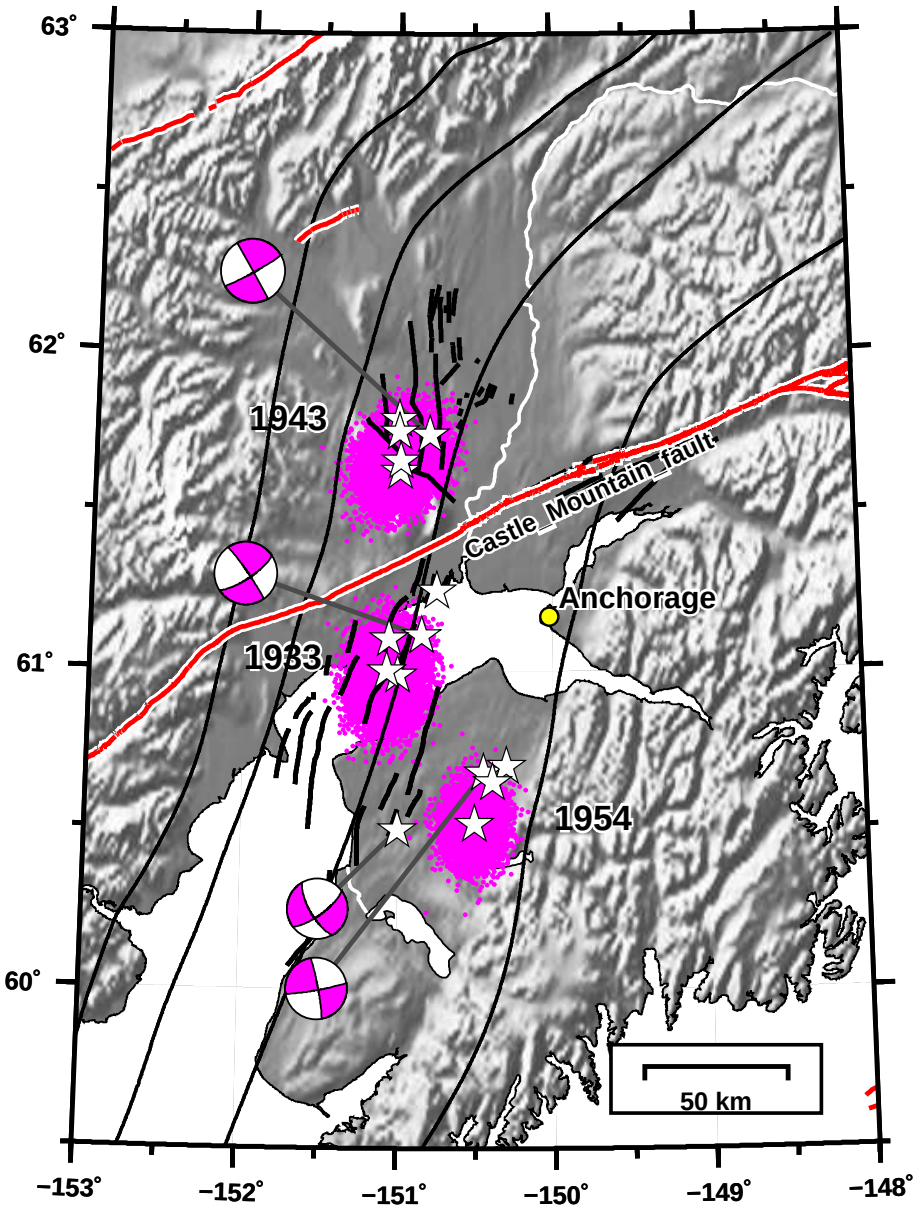

Figure 3: Estimated epicenters for the 1933, 1943 and 1954 earthquakes. Each cloud of colored dots represents the posterior epicenters, which are centered on a maximum likelihood epicenter (star). Other stars show epicenter estimates from other studies (*Engdahl and Villasenor*, 2002; *Doser and Brown*, 2001; *Gutenberg and Richter*, 1954; *Storchak et al.*, 2013). See Figure 4 for information regarding the depths of the posterior samples relative to the underlying subduction interface. Also shown are active faults and folds (*Koehler et al.*, 2012; *Haeussler et al.*, 2017) and contours of the top of the subducting Pacific plate (40 km, 60 km, 80 km, 100 km) (*Li et al.*, 2013). The beachballs show three focal mechanisms estimated from *Doser and Brown* (2001) and one (1954) from *Wickens and Hodgson* (1967).

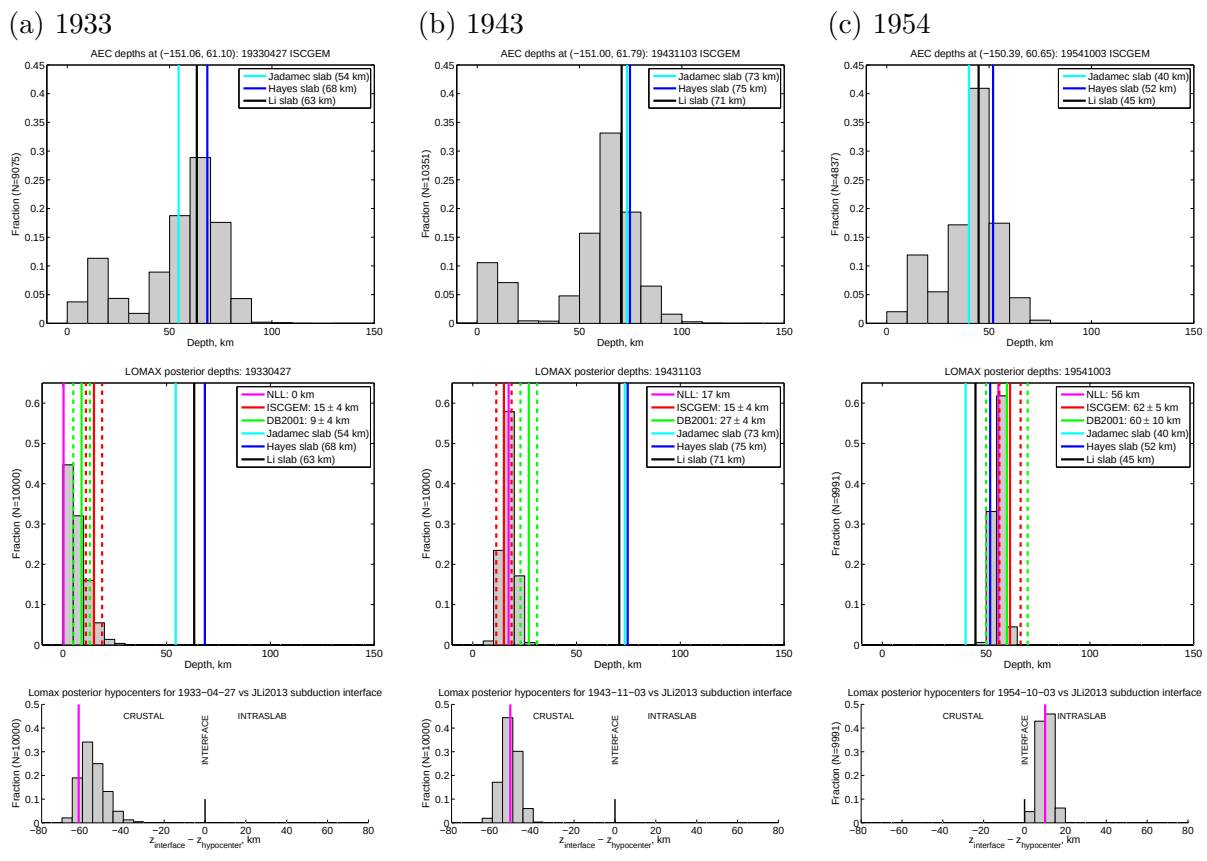

Figure 4: Estimated depth to slab for three historical earthquakes. Each hypocentral estimation using NonLinLoc provides a cloud of posterior hypocenters; see Figure 3 for a map view. For each posterior hypocenter we evaluate the vertical distance to the subduction interface models of *Jadamec and Billen* (2010) (cyan), *Hayes et al.* (2012) (blue), and *Li et al.* (2013) (black). (a) 1933-04-27 M_{w} 6.8 earthquake. (top) Distribution of depths of modern microseismicity ($M \geq 0$, 2000–2018) whose epicenters are within a 40 km of the ISC-GEM epicenter. (middle) Distribution of depths of posterior hypocenters. Also shown are our maximum-likelihood estimate from NonLinLoc (magenta) and the depth estimates, with uncertainties, from ISC-GEM (*Storchak et al.*, 2013) (red) and DB2001 (*Doser and Brown*, 2001) (green). (bottom) Distribution of vertical distances between our posterior hypocenters and the underlying subduction interface from *Li et al.* (2013). Distributions to the left favor a crustal interpretation for the earthquake; distributions to the right favor an intraslab interpretation. (b) 1943-11-03 M_{w} 7.3 earthquake. (c) 1954-10-03 M_{w} 6.4 earthquake.

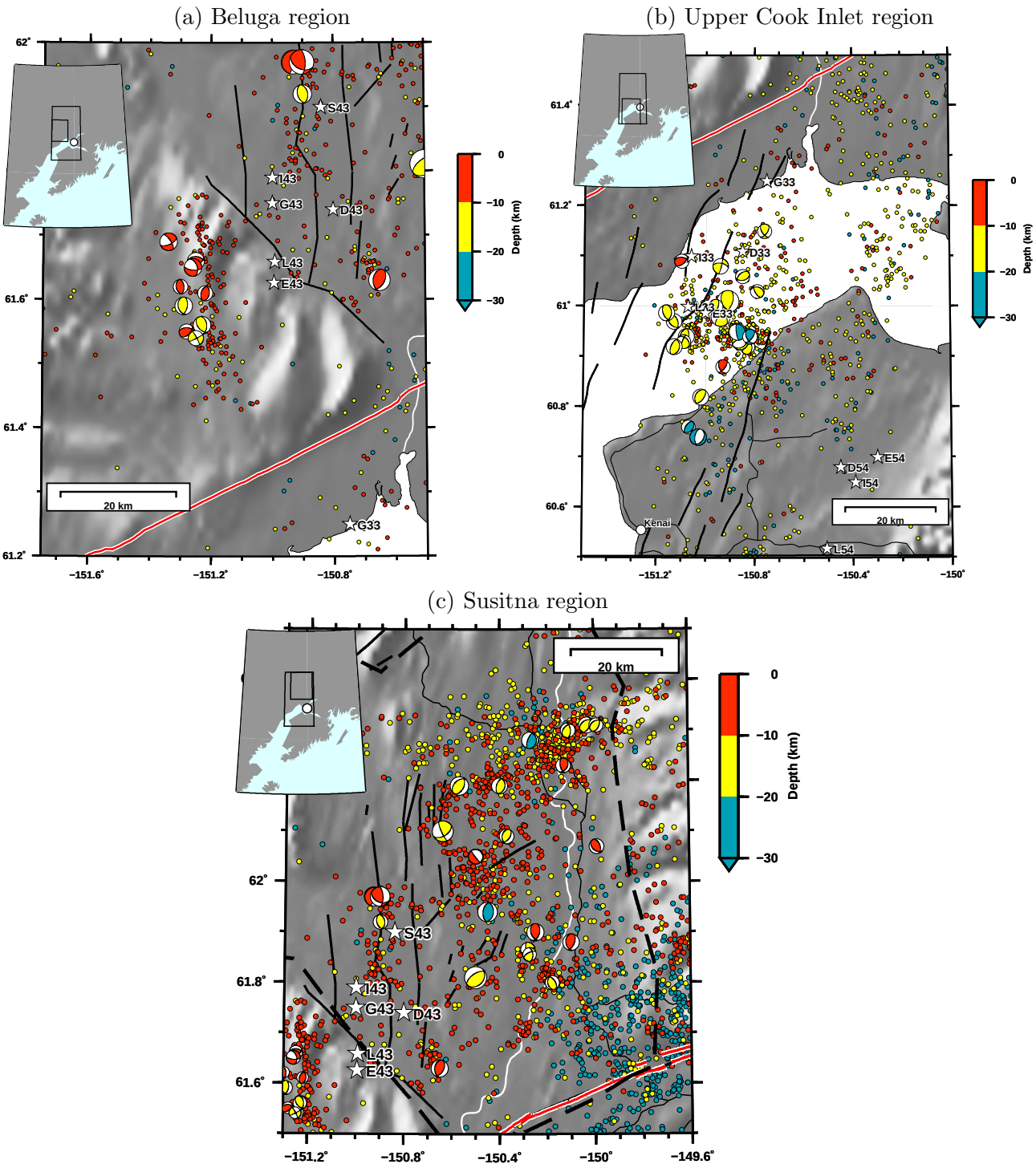

Figure 5: Our double couple moment tensor solutions for crustal earthquakes (depth $\leq$ 30 km) between 2007-08-15 and 2017-01-01 in three focus regions (Table 1). Beachballs size is scaled by earthquake magnitude, and colored by depth. Also shown are relocated seismicity (Figure 6) and previously published epicenters for the 1933 and 1943 earthquakes, plotted as stars. In the inset map, the smaller (inner) bounded reigon represents the subregion and the outer bounds represents the full study region. (a) $M_w \geq 2.5$ in the Upper Cook Inlet region. (b) $M_w \geq 2.5$ in the Beluga region. (c) $M_w \geq 3.0$ in the Susitna region.

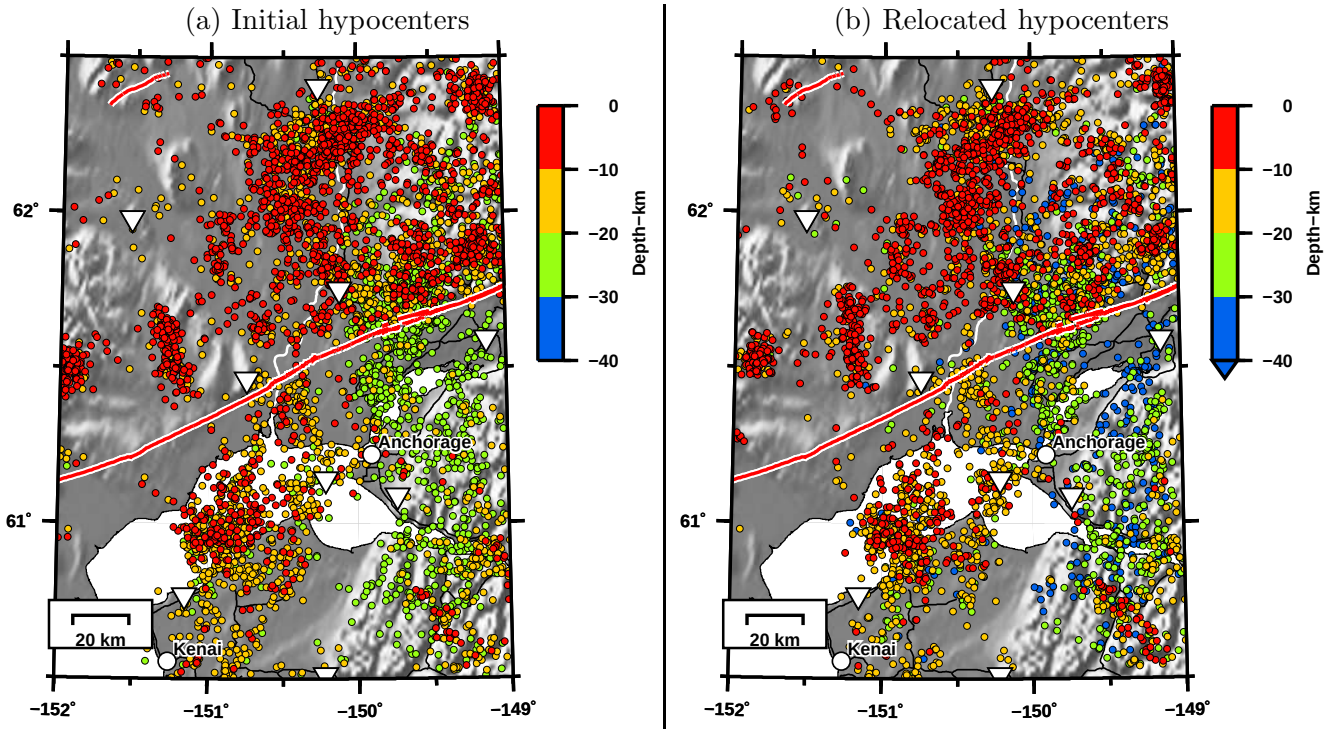

Figure 6: Relocation of hypocenters using a double-difference approach. The crustal earthquakes considered have depth ≤ 30 km, $M_{\mathrm{w}} \geq 1.5$, and occurred between 1990-01-01 and 2017-01-01.